



ORIGINAL ARTICLE

Gold nanoparticle encoded with marigold (*Tagetes erecta* L.) suppressed hyperglycemia -induced senescence in retinal pigment epithelium via suppression of lipid peroxidation



Sun Young Park ^{a,*}, Kangmin Park ^a, Jin-Woo Oh ^b, Geuntae Park ^{b,*}

^a *Bio-IT Fusion Technology Research Institute, Pusan National University, Geumjeong-gu, Busan 46241, Republic of Korea*

^b *Department of Nanomaterials Engineering, Pusan National University, Geumjeong-gu, Busan 46241, Republic of Korea*

Received 1 June 2023; accepted 29 June 2023

Available online 4 July 2023

KEYWORDS

Marigold;
Gold nanoparticle;
Retinal pigment epithelium;
Senescence;
Lipid peroxidation

Abstract This paper presents a simple and environmentally friendly method for synthesizing *Tagetes erecta* L. gold nanoparticles (TE-GNPs) using an aqueous extract of *Tagetes erecta* L. (TE). The TE extract serves as a reducing and stabilizing agent, and its antioxidant activity is evaluated using 2,2'-azino-bis(3-ethylbenzothiazoline-6-sulfonic acid) (ABTS) and 2,2-diphenyl-1-picrylhydrazyl (DPPH) assays. The TE extract exhibits significant DPPH and ABTS radical scavenging activities, indicating its strong antioxidative properties attributed to various antioxidant compounds. TE-GNPs are successfully synthesized by incubating the TE extract with a chloroauric acid solution, resulting in a color change from light yellow to ruby red. UV-Vis spectroscopy confirms the synthesis of TE-GNPs, evidenced by a characteristic absorption peak at approximately 524 nm, corresponding to the nanoparticles' surface plasmon resonance. Physicochemical characterization reveals that TE-GNPs possess nanoscale dimensions (28.9 ± 2.3 nm), stability (zeta potential of -31.5 ± 28), and a crystalline nature (validated via X-ray diffraction; XRD). Functional groups responsible for biosynthesis and stabilization are identified through Fourier transform infrared spectroscopy (FT-IR) analysis. high-resolution transmission electron microscopy (HR-TEM) images demonstrate the morphology, size, and dispersion of TE-GNPs, while selected area electron diffraction (SAED) patterns confirm their crystalline structures. Additionally, high-angle annular dark field (HAADF) imaging and energy-dispersive X-ray spectroscopy (EDX) spectroscopy verify the distri-

* Corresponding authors at: Department of Nanofusion Technology, Graduate School, Pusan National University, Busan 46241, Republic of Korea (G. Park), Bio-IT Fusion Technology Research Institute, Pusan National University, 2, Busandaehak-ro 63beon-gil, Geumjeong-gu, Busan 46241, Republic of Korea (S.Y. Park).

E-mail addresses: sundeng99@pusan.ac.kr (S. Young Park), gtpark@pusan.ac.kr (G. Park).

Peer review under responsibility of King Saud University.



Production and hosting by Elsevier

bution and presence of gold in the TE-GNPs, respectively. Cytotoxicity assays confirm the biocompatibility of TE-GNPs. Furthermore, their potential in mitigating high glucose-induced cell death and oxidative stress in retinal pigment epithelial (RPE) cells is evaluated. Treatment with TE-GNPs restores the proliferation rate of RPE cells and reduces the proportion of apoptotic cells under high glucose conditions. TE-GNPs also decrease the high glucose-induced production of intracellular and mitochondrial reactive oxygen species. Markers of cellular senescence, including SA- β -galactosidase activity and lysosomal dysfunction, are attenuated by the TE-GNPs. Moreover, the TE-GNPs effectively reduce lipid accumulation and peroxidation in RPE cells exposed to high levels of glucose. These findings highlight the successful green synthesis of TE-GNPs using an aqueous extract of TE and underscore their desirable properties and anti-senescence effects.

© 2023 The Author(s). Published by Elsevier B.V. on behalf of King Saud University. This is an open access article under the CC BY-NC-ND license (<http://creativecommons.org/licenses/by-nc-nd/4.0/>).

1. Introduction

Nanotechnology allows public health and environmental challenges to be addressed sustainably through research and manufacturing. Nanomaterials possess unique physicochemical properties that render them ideal for various technical applications, e.g., their small size, crystalline surface, chemical composition, shape, and solubility (Sarfraz and Khan, 2021, Rodrigues et al., 2017, Salem et al., 2022). Conventional physical and chemical manufacturing methods, such as thermal decomposition, laser irradiation, and electrolysis, require advanced technology and considerable energy. Chemical synthesis methods, such as chemical reduction, present some limitations owing to the use of hazardous chemicals, the requirement for high temperatures and pressures, and the production of toxic byproducts (Shreyash et al., 2021a, Ali et al., 2016, Sampath et al., 2022). Alternatively, biological approaches for synthesizing nanoparticles using bacterial, fungal, yeast, viral, and plant biomass/extracts are becoming increasingly popular owing to their environmentally friendly nature. Among these methods, plant-mediated biosynthesis indicates potential for synthesizing metal nanoparticles from biomolecules, such as proteins, vitamins, enzymes, polysaccharides, amino acids, and organic acids such as citric acid, which are present in plant biomass. This method has been used for waste management and dye reduction, thus rendering it a compelling option for sustainable research and manufacturing (Al-Radadi, 2021, Anwar et al., 2021, Hassan et al., 2022). The synthesis of nanoparticles using plant extracts is a promising, cost-effective, and environmentally friendly alternative to chemical synthesis. Various metal salts, such as Ag, Au, Pt, and Pd, can be reduced and converted into nanomaterials using different methods (Jeevanandam et al., 2022, Kouhpanji and Stadler, 2020). Plant extracts contain various reducing agents such as sugars, flavonoids, phenolic acids, terpenoids, and polyphenols, which can transform metal atoms and ions into nanoscale materials. Plant-mediated biosynthesis of metal nanoparticles has become increasingly popular owing to its speed, safety, nonpathogenicity, and environmental friendliness. Compared with conventional chemical or physical methods, green synthesis involves fewer steps, requires minimal energy, pressure, and temperature, and is highly energy-efficient and cost-effective for large-scale production. Biologically active plant components serve as reducing and stabilizing agents, which renders them ideal for nanoparticle synthesis (Jeevanandam et al., 2022, Prakash et al., 2022, Patil and Chandrasekaran, 2020).

Diabetic retinopathy (DR) is a chronic condition characterized by vision loss that primarily results from dysfunction and damage to the retinal pigment epithelium (RPE). The development and progression of DR are closely associated with oxidative stress caused by the accumulation of reactive oxygen species (ROS) triggered by hyperglycemia. However, the specific cellular mechanisms that correlate ROS, oxidative stress, and RPE pathology in DR are yet to be elucidated (Lima et al., 2022, Nolan et al., 2021). Recent studies have provided some insights into the potential role of cellular senescence, which is a state of irreversible growth arrest induced by sub-lethal levels of ROS, in DR.

Although high glucose levels have been shown to induce cellular senescence in various cell types, its effect on RPE senescence, specifically in DR, has not been investigated comprehensively (Chen et al., 2019, Lee, E. J. et al., 2022, Tohari et al., 2020). RPE cells are particularly vulnerable to oxidative damage due to exposure to high oxygen levels and continuous light stimulation. Meanwhile, widespread RPE cell death is not typically observed in the early stages of DR, suggesting that cellular senescence may represent an early response to oxidative stress in the RPE. Furthermore, disruptions in lipid homeostasis have been implicated in age-related diseases, including DR (Nolan et al., 2021, Seo et al., 2019, Lee, E. J. et al., 2022). Lipid metabolism may result in the generation of oxidant species, and alterations in lipid metabolism have been observed in RPE cells under oxidative stress. However, the precise role of lipids in RPE dysfunction and their relationship with DR remains unclear. Understanding the intricate relationship among oxidative stress, cellular senescence, and lipid metabolism in RPE dysfunction is crucial to understand the pathogenesis of DR and develop targeted interventions. By understanding these mechanisms, effective therapeutic strategies to prevent or manage DR can be further developed.

Marigold (*Tagetes erecta* L.) is a flowering plant belonging to the Asteraceae family and is cultivated globally, with significant production in Mexico, Peru, Spain, India, and China. This plant is traditionally recognized for its medicinal properties and is typically referred to as smelly hibiscus or gold chrysanthemum. Marigold flowers have been used for centuries to treat various ailments, including fever, epilepsy, stomachic issues, scabies, liver ailments, and eye disorders (Zhang et al., 2020, Meurer, Mariane et al., 2022, Meurer, Marianne Caroline et al., 2019). Green chemistry methods have received considerable attention owing to their environmentally friendly nature and sustainability. Hence, green synthesis methods are preferred for producing nanoparticles. In this context, marigold has emerged as a promising candidate for nanoparticle synthesis owing to its natural abundance and rich content of bioactive compounds. Marigold flowers are a rich source of natural carotenoids, among which lutein and zeaxanthin are the most abundant. These carotenoids possess antioxidant properties and are associated with various health benefits, particularly eye health. In particular, lutein has been associated with a reduced risk of age-related macular degeneration and visual impairment, as well as the overall health of the eyes and skin. In addition to being a natural colorant, marigold-derived lutein can be used in other applications. Its various biological properties, including antioxidant, antibacterial, antidiabetic, anti-obesity, anti-inflammatory, and anticancer effects, have received significant scientific interest (Shamarao and Chethankumar, 2022, Wang et al., 2006, Fernández-Sevilla et al., 2010, Gansukh et al., 2019). The focus of this study is to investigate the synthesis of gold marigold nanoparticles (TE-GNPs) using a green approach. We aim to explore the reduction potential of marigold extract for converting gold ions into nanoparticles and optimize the synthesis process for efficient and environmentally sustainable nanoparticle production. Additionally, we aim to evaluate the effects of TE-GNPs on hyperglycemia-induced premature senescence in RPE cells.

2. Material and methods

2.1. Preparation of TE extract

Tagetes erecta (TE) flowers were obtained from Kwang Myoung Herb Medicine, a local herbal store in Pusan, South Korea. Dr. Young Whan Choi from Pusan National University conducted the botanical identification, and a voucher specimen (no. MT20210007) was deposited at the Natural Products Research Laboratory of the university. To extract the active components, 300 g of dried TE roots were boiled in distilled water at 100 °C for 4 h. The resulting extract was then filtered through a 0.45 µm filter, freeze-dried (yield = 27 g), and stored at 4 °C. Prior to use, the dried extract was dissolved in phosphate-buffered saline (PBS) and filtered through a 0.22 µm filter.

2.2. Analysis of DPPH and ABTS free radical scavenging activities of TE extract

The DPPH and ABTS radical scavenging activities of the TE extract were evaluated using modified protocols. The TE extract and a 60 µM solution of DPPH in ethanol (Sigma-Aldrich–Merck KGaA, Burlington, MA, USA) were mixed in equal volumes and allowed to react in the dark at room temperature (22 °C–25 °C) for 30 min. The absorbance was measured at 510 nm using a VICTOR Multilabel Plate Reader to assess the DPPH activity. For the ABTS assay, stock solutions of 7 mM ABTS (Sigma-Aldrich–Merck KGaA, Burlington, MA, USA) and 2.6 mM potassium persulfate (Sigma-Aldrich–Merck KGaA, Burlington, MA, USA) were prepared in double distilled water at room temperature (22–25 °C) in the dark for 16 h. The TE extract was mixed with the ABTS solution and incubated in darkness at room temperature for 30 min. The absorbance was measured at 734 nm using an Ultrospec 6300 Pro (GE Healthcare Life Sciences, Buckinghamshire, UK) to evaluate the ABTS activity.

2.3. Green synthesis of TE-GNPs

TE-GNPs were synthesized using a modified reduction method with chloroauric acid. Initially, a 1 mM HAuCl₄ (Sigma-Aldrich–Merck KGaA, Burlington, MA, USA) solution was mixed with the TE-GNP extract and incubated at 25 °C and 200 rpm for 15 min. Undesired components were separated by centrifugation at 13,000 rpm for 20 min, followed by three rounds of washing with deionized water to remove any remaining residues. The purified TE-GNPs were characterized using UV–Vis spectrophotometry (Ultrospec 6300 Pro) to confirm their presence in the 300–800 nm wavelength range. The size and zeta potential of the nanoparticles were determined by dynamic light scattering (Zetasizer Nano ZS90) with data transfer assistance software.

2.4. Physicochemical characterization of TE-GNPs

The physicochemical characterization of TE-GNPs included X-ray diffraction (XRD) and Fourier transform infrared (FTIR) analyses. XRD patterns were obtained using an X-ray diffractometer (XRD Empyrean Series 2, PANalytical,

Almelo, Netherlands) to determine the crystalline structures of the TE extracts and TE-GNPs. FTIR spectra were recorded using an FTIR spectrophotometer (Spectrum GX, PerkinElmer Inc., Boston, MA, USA) in the range of 4000–400 cm⁻¹ to identify the various functional groups involved and analyze the formation of gold nanoparticles. The morphological features and sizes of the synthesized TE-GNPs were determined using high-resolution transmission electron microscopy (HR-TEM) (TALOS F200X, FEI, Oregon, USA) and selected area electron diffraction (SAED). The crystalline nature of TE-GNPs was confirmed by comparing the SAED pattern with the HR-TEM data. The composition of TE-GNPs was analyzed using energy-dispersive X-ray spectroscopy (EDS) on a TALOS F200X HR-TEM equipped with a dispersive X-ray spectrometer. The experimental procedures were conducted following standard protocols.

2.5. RPE cell culture and treatment

The ARPE-19 human RPE cell line obtained from the American Type Culture Collection (ATCC, Manassas, VA, USA) was cultured in DMEM/F12 supplemented with 10% fetal bovine serum and 1% penicillin–streptomycin (GIBCO, Grand Island, NY, USA). The cells were maintained at 37 °C with 5% CO₂ in a humidified atmosphere. Experiments were conducted using cells in 15–20 passages. To induce senescence, the RPE cells were initially cultured in a low-glucose medium until 80% confluency. Subsequently, they were immersed in a high-glucose medium for 48 h after a 24-h serum-free period. For treatment experiments, the RPE cells were seeded in 24-well plates or 6 cm Petri dishes at a density of 5 × 10⁴ cells/mL and incubated overnight. Subsequently, the cells were subjected to various concentrations (25, 50, 100, and 200 µg/mL) of TG-GNPs in a serum-free medium for a duration of 24 h. Subsequently, the cells were exposed to 30 mM D-glucose (referred to as high glucose, HG) for an additional 48 h. As for the control group (normal glucose), RPE cells were cultured in a medium containing 5.5 mmol/L D-glucose and 24.5 mmol/L mannitol.

2.6. CCK-8 for RPE cell viability

To evaluate the viability of the RPE cells, we used a Cell Counting Kit 8 (CCK-8) from Sigma-Aldrich–Merck KGaA (Burlington, MA, USA). Briefly, 2 × 10⁴ cells were seeded into each well of a 96-well plate and treated with various compounds. Subsequently, 20 µL of the CCK-8 solution was added to each well, followed by incubation at 37 °C for 3 h. The absorbance of the samples was measured at 450 nm using a microplate reader provided by Perkin–Elmer (Waltham, MA, USA).

2.7. Dual Annexin-V and PI staining assay for assessing RPE cell death

RPE cell apoptosis was assessed using the Dead Cell Apoptosis Kit with Annexin V Alexa Fluor 488 and propidium iodide (PI) (Invitrogen, Carlsbad, CA, USA) and quantified using a flow cytometer (Beckman Coulter FC500, Pasadena, CA, USA) based on the manufacturer's recommended protocols. The distribution of cells in the upper left, lower left, upper

right, and lower right quadrants corresponded to damaged cells (Annexin V-, PI +), viable cells (Annexin V-, PI-), RPE cells in late apoptosis (Annexin V+, PI +), and RPE cells in early apoptosis (Annexin V+, PI-), respectively.

2.8. Intracellular reactive oxygen species (ROS) and mitochondrial ROS assay

Intracellular ROS were measured by quantifying the conversion of CM-H2DCFDA (Thermo Fisher Scientific) to fluorescent DCF. The RPE cells were treated with 2 μ M CM-H2DCFDA for 20 min at 37 °C in the dark; subsequently, they were washed with a serum-free cell culture medium. Flow cytometry was performed using a Beckman Coulter FC500 flow cytometer (Pasadena, CA, USA) and analyzed using the CXP Software (version 1.2). To assess their mitochondrial ROS levels, the RPE cells were exposed to MitoSOX Red (5 μ M) for 10 min at 37 °C, followed by incubation for 30 min using Hoechst 33,342 (Thermo Fisher Scientific, Waltham, MA, USA). Fluorescent signals were captured and quantified using a confocal microscope (LSM 800; Carl Zeiss, Jena, Germany).

2.9. Assessment of senescence-associated β -galactosidase (SA- β -gal) activity

SA- β -gal activity was determined using a senescence-galactosidase staining kit (Cell Signaling Technology, Beverly, MA, USA) and a quantitative cellular senescence assay kit (Cell Biolabs, Inc., San Diego, CA, USA) based on the manufacturer's instructions. To quantify SA- β -gal activity, the percentage of SA- β -gal-stained RPE cells relative to the total number of RPE cells counted in the optical field was determined. The fluorescence intensity of the stained cells was measured using a flow cytometer (Beckman Coulter FC500, Pasadena, CA, USA).

2.10. Assessment of lysosome content

The intracellular lysosome content in the RPE cells was evaluated using LysoTracker Green DND-26 dye (Cell Signaling Technology, Beverly, MA, USA) based on the manufacturer's instructions. The RPE cells were washed with PBS and subsequently incubated with LysoTracker Green DND-26 in a light-protected environment for 30 min. The fluorescence intensity emitted by the LysoTracker Green dye was used to measure the lysosome content in the cells. To quantify the lysosomal content, the fluorescence intensity was analyzed using a flow cytometer (Beckman Coulter FC500, Pasadena, CA, USA).

2.11. Assessments of lipid accumulation

To assess the lipid droplets, the RPE cells were stained using an Oil Red O staining kit (BioVision, Milpitas, CA, United States). The RPE cells were washed twice with phosphate-buffered saline, followed by fixation with 10% formalin. Subsequently, the cells were stained with Oil Red O solution for 1 h at room temperature. After the incubation period, the Oil Red O staining solution was removed and images of the stained lipid droplets were captured using an optical micro-

scope. To quantify the lipid droplets, the remaining Oil Red O staining reagent within the cells was dissolved in isopropanol and then separated. The absorbance of the resulting solution was measured at 490 nm.

2.12. Assessments of intracellular lipid peroxidation

Lipid peroxidation was evaluated using BODIPY 581–591 C11 dye (Thermo Fisher Scientific, Waltham, MA, USA). The RPE cells were treated with 0.5 μ M BODIPY 581–591 C11 and incubated for 30 min at 37 °C. To assess lipid peroxidation, an LSM 800 confocal microscope (Carl Zeiss, Jena, Germany) equipped with a 40x water-immersion objective was used. The resulting data were processed using the CXP Software (version 1.2).

2.13. Statistical analysis

In-vitro experiments were conducted in triplicate and repeated at least thrice. The data were presented as the mean \pm SE with individual data points. The one-way ANOVA followed by Dunn's post-hoc test were performed for statistical analysis. Differences were considered statistically significant at $p < 0.05$, which indicates significant differences between groups or conditions.

3. Results

3.1. Physicochemical characterization of TE-GNPs

The physicochemical characterization of TE-GNPs was conducted to assess their properties. The TE extract demonstrated significant antioxidant activity, as indicated by the DPPH and ABTS radical scavenging assays, with scavenging activity ranging from 7.3% to 98.9%. This activity can be attributed to the presence of various antioxidant compounds in the TE extract (Fig. 1A). The successful green synthesis of TE-GNPs was confirmed through visual observation of a color change from light yellow to ruby red upon incubation of the TE extract with a chloroauric acid solution. UV-Vis spectroscopy further confirmed the synthesis, showing a characteristic absorption peak at approximately 524 nm, corresponding to the surface plasmon resonance of the nanoparticles (Fig. 1B). Scattering methods were employed to analyze the size, zeta potential, and polydispersity of the TE-GNPs. The average size of the TE-GNPs was measured to be 28.9 ± 2.3 nm, indicating their nanoscale dimensions (Fig. 1C). Zeta potential analysis revealed stable values of -31.5 ± 28 , indicating the stability of the TE-GNPs (Fig. 1D). XRD measurements confirmed the crystalline nature of the TE-GNPs, with well-defined diffraction peaks at (111), (200), (220), and (311), indicating a highly purified composition of crystalline gold in the synthesized nanoparticles (Fig. 1E). FTIR analysis provided insights into the functional groups contributing to the reduction and stabilization of the TE-GNPs. Specific peaks observed at wavenumbers 3329.07 and 1343.31 cm^{-1} corresponded to –OH bond stretching alcohols or polyphenol, while the peak at 795.09 cm^{-1} was attributed to C-N amide bending inorganic carbonates. These functional groups are vital to the biosynthesis and stabilization of the TE-GNPs

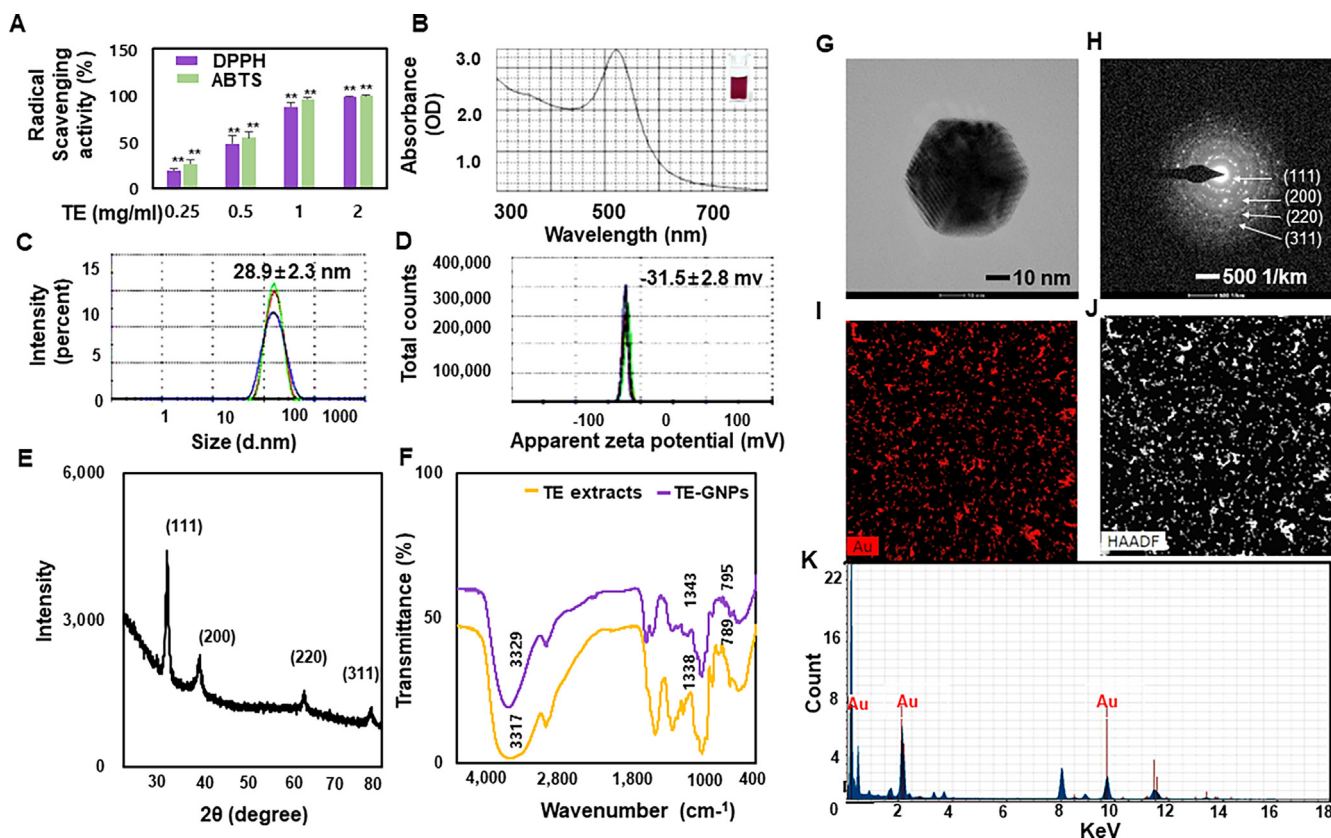


Fig. 1 Antioxidant activity and physicochemical characterization of TE-GNPs. (A) DPPH and ABTS radical scavenging activities of TE extract. (B) UV-Vis spectroscopy analysis of green-synthesized TE-GNPs. (C) Hydrodynamic size of TE-GNPs determined via DLS. (D) Zeta potential of TE-GNPs measured via DLS. (E) XRD patterns of synthesized TE-GNPs. (F) FTIR spectra of TE extract and synthesized TE-GNPs. (G) Particle shape of TE-GNPs observed via HR-TEM. (H) SAED pattern confirming crystalline structure of TE-GNPs. (I, J) HAADF images showing distribution of gold in TE-GNPs. (K) EDS analysis confirming presence of gold peaks. Data are presented as mean \pm standard error (SE) of three independent experiments, and statistical significance is indicated by ## $p < 0.05$ and ** $p < 0.01$.

(Fig. 1F). HR-TEM analysis allowed for high-resolution observation of the TE-GNPs, revealing their shape, size, and dispersion. TEM images showed TE-GNPs with diameters ranging from approximately 5.46 nm to 24.39 nm (Fig. 1G). The SAED pattern confirmed the crystalline structure of the TE-GNPs, displaying distinct lattice planes (Fig. 1H). Furthermore, HAADF imaging provided visual evidence of the distribution of gold in the TE-GNPs (Fig. 1I and J), and EDX spectroscopy confirmed the presence of gold peaks in the TE-GNPs spectra (Fig. 1K). These results indicate the successful synthesis of gold nanoparticles using the TE extract. The characterized TE-GNPs possessed desirable properties, including strong antioxidative activity, nanoscale size, stability, crystallinity, and well-defined morphology.

3.2. Protective effect of TE-GNPs against high glucose-induced RPE dysfunction

To assess the protective effect of TE-GNPs, we first evaluated their cytotoxicity in RPE cells under normal and high-glucose conditions. The RPE cells were treated with varying concentrations of TE-GNPs for 2 h before exposure to high glucose (30 mM). Cell viability was measured using the CCK-8 assay to assess the proliferative ability of RPE cells under different

conditions. Under normal conditions, treatment with TE-GNPs at concentrations ranging from 25 to 200 $\mu\text{g}/\text{mL}$ did not significantly affect the cell viability of RPE cells, indicating their biocompatibility (Fig. 1A). However, under high glucose conditions, the proliferative ability of RPE cells was significantly impaired compared to normal conditions. Remarkably, treatment with TE-GNPs restored the proliferation rate of RPE cells, suggesting their protective effect against high glucose-induced dysfunction (Fig. 2A). To further investigate the impact of TE-GNPs on cell death in RPE cells exposed to high glucose, we conducted Annexin V/PI staining. This assay detects cell death by binding Annexin V to phosphatidylserine exposed on the outer membrane of apoptotic or dying cells, while PI enters cells with compromised plasma membranes, indicating late-stage cell death (Tohari et al., 2020). Flow cytometry analysis revealed a significant increase in the proportion of RPE cells exhibiting double-positive staining for activated Annexin V and PI under high glucose conditions. However, treatment with TE-GNPs significantly reduced the proportion of double-positive cells compared to the high glucose group, indicating their ability to alleviate cell death (Fig. 2B). Oxidative stress plays a crucial role in retinal damage and the pathogenesis of RPE cell death (Tang et al., 2022). To evaluate the effect of TE-GNPs on high glucose-induced oxidative stress, we measured intracellular reactive

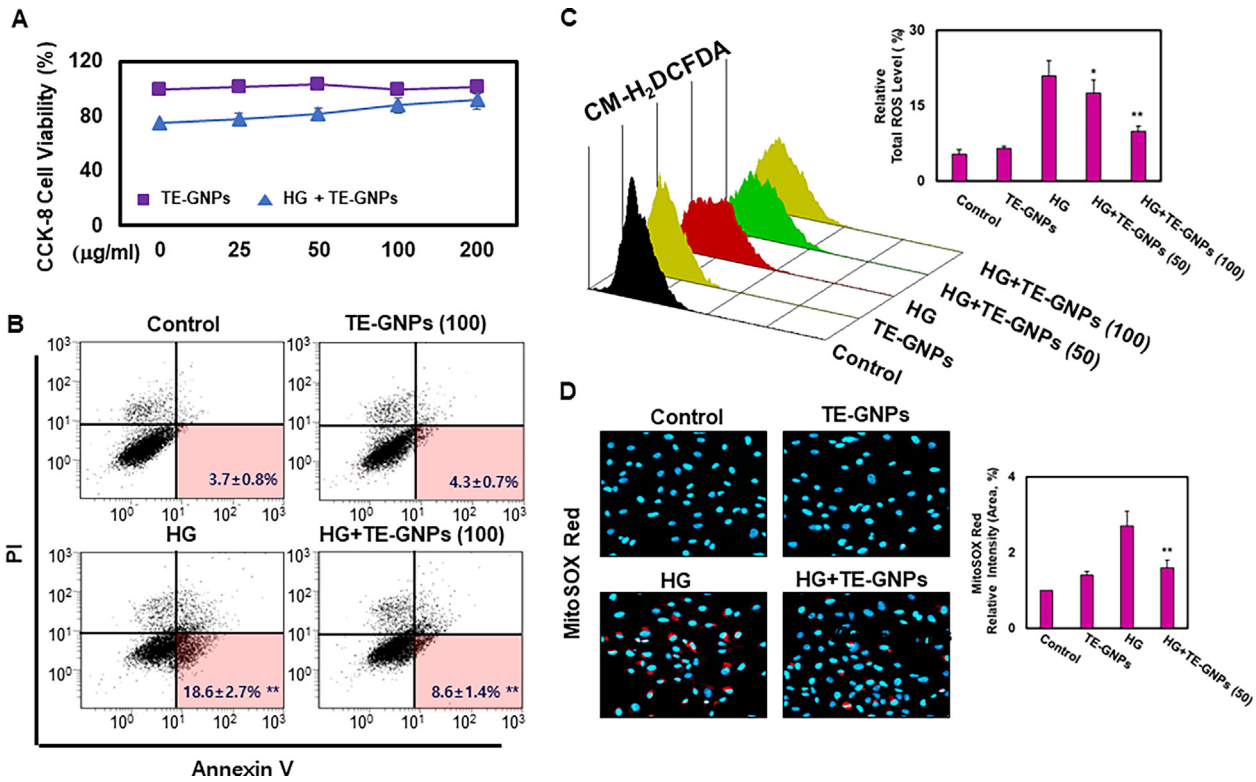


Fig. 2 Effects of TE-GNPs on apoptosis and ROS levels in high glucose-cultured RPE cells. (A) Effect of TE-GNPs on proliferation rates of RPE cells under normal and high glucose conditions. (B) Effect of TE-GNPs on apoptosis rates of RPE cells under normal and high glucose conditions. (C) Effect of TE-GNPs on intracellular ROS levels in RPE cells under normal and high glucose conditions. (D) Effect of TE-GNPs on mitochondrial ROS levels in RPE cells under normal and high glucose conditions. Data represent mean \pm standard error (SE) from three independent experiments. Statistical significance is indicated by ## $p < 0.05$ and ** $p < 0.01$.

oxygen species (ROS) levels using the cell-permeable H2DCFDA fluorescence probe. RPE cells exposed to high glucose exhibited a significant increase in intracellular ROS accumulation, indicating oxidative damage. However, treatment with TE-GNPs significantly reduced the levels of intracellular ROS induced by high glucose, demonstrating their antioxidative properties (Fig. 2C). Additionally, mitochondrial ROS generation was assessed using MitoSOX Red dye and confocal microscopy. RPE cells exposed to high glucose showed an elevated MitoSOX Red fluorescence signal, indicating increased mitochondrial ROS production (Fig. 2D). In contrast, treatment with TE-GNPs significantly decreased the fluorescence intensity of MitoSOX Red in high glucose-exposed RPE cells, indicating their ability to mitigate mitochondrial ROS generation (Fig. 2D).

3.3. Prevention of high glucose-induced RPE senescence by TE-GNPs

We investigated the effects of TE-GNPs on cellular senescence using a cellular model of high-glucose-cultured RPE cells. Cellular senescence is characterized by irreversible growth arrest and various molecular and phenotypic changes. Lysosomal dysfunction and increased SA- β -galactosidase (SA- β -gal) activity are two key markers associated with cellular senescence (Lee, K. S. et al., 2021, Ren et al., 2022). In our study, we observed a significant increase in SA- β -gal activity in RPE cells exposed to high glucose compared to the control

group, indicating an enhanced senescence phenotype (Fig. 3A). However, pre-exposure of RPE cells to TE-GNPs significantly reduced SA- β -gal activity, suggesting a preventive effect against high glucose-induced cellular senescence. To quantitatively assess cellular senescence, we performed flow cytometry analysis using SA- β -gal staining. High-glucose-cultured RPE cells exhibited a substantial increase in SA- β -gal staining levels, indicative of an enhanced senescence phenotype compared to the control group (Fig. 3B). However, pretreatment with TE-GNPs inhibited the high glucose-induced increase in SA- β -gal activity, suggesting their ability to mitigate cellular senescence. In the context of cellular senescence, we also investigated the effect of TE-GNPs on lysosomal content using LysoTracker Green DND-26 staining and flow cytometry. The results demonstrated a significant increase in lysosomal content in high-glucose-cultured RPE cells compared to the control group (Fig. 3C). However, pretreatment with TE-GNPs effectively reduced the lysosomal content in high-glucose-cultured RPE cells, indicating their potential to alleviate lysosomal dysfunction associated with cellular senescence induced by high glucose.

3.4. Effect of TE-GNPs on high glucose-induced lipid accumulation and peroxidation

To investigate whether RPE cells respond to high glucose levels by accumulating lipids, we performed Oil Red O staining, a selective method for detecting neutral lipids, specifically

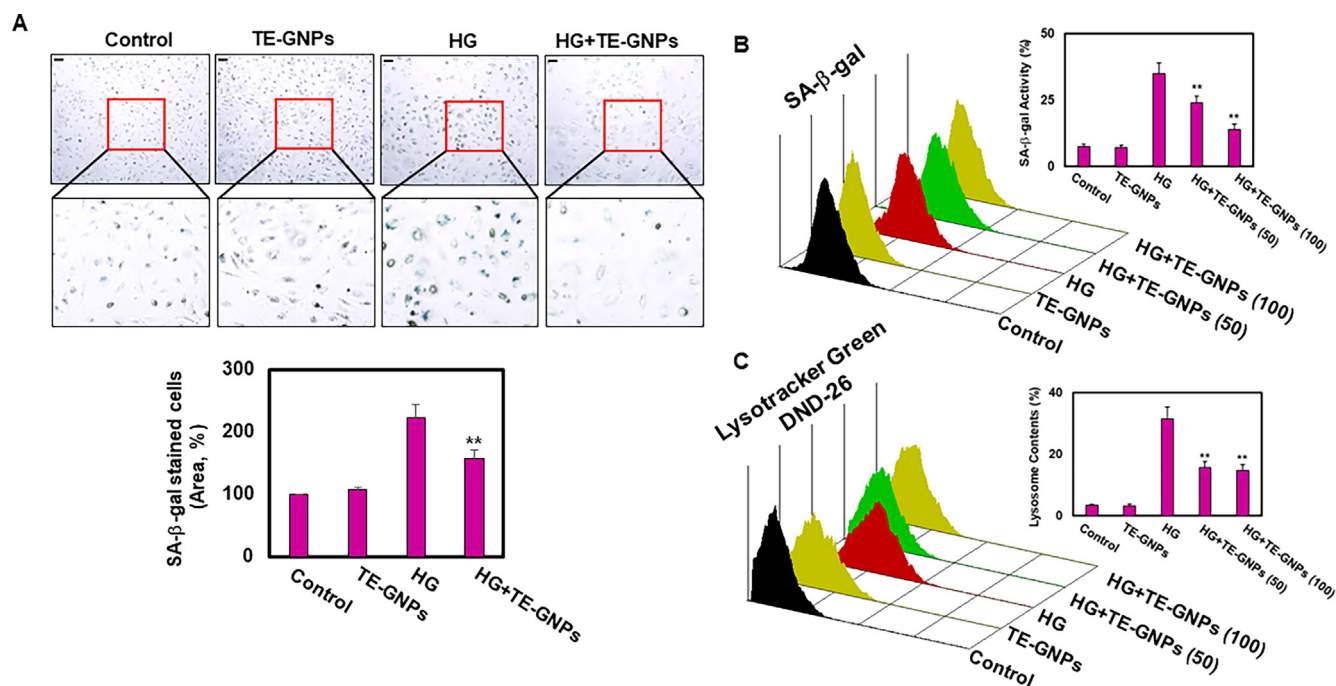


Fig. 3 Effects of TE-GNPs on SA-β-galactosidase activity and lysosomal content in high glucose-cultured RPE Cells. (A) Visualization of SA-β-galactosidase activity achieved using Senescence β-Galactosidase Staining Kit. (B) Quantification of SA-β-galactosidase activity performed using Quantitative Cellular Senescence Assay Kit. (C) Flow cytometry analysis using LysoTracker Green DND-26 staining for evaluating lysosomal content in RPE cells. Data represent the mean ± standard error (SE) from three independent experiments. Statistical significance is indicated by ###p < 0.05 and **p < 0.01.

triglycerides stored within lipid droplets. After a 48-hour exposure to high glucose, RPE cells exhibited an increased intensity of Oil Red O staining, indicating elevated lipid accumulation (Fig. 4A). However, pretreatment with TE-GNPs significantly reduced the intensity of Oil Red O staining, suggesting that TE-GNPs effectively reduced lipid accumulation in RPE cells exposed to high glucose concentrations. Lipid peroxidation plays a crucial role in cellular senescence as it leads to the generation of reactive lipid species that cause cellular damage (Seo et al., 2019). To assess lipid peroxidation, we utilized the BODIPY-581/591 C11 probe, which emits green fluorescence in its reduced form and red fluorescence in its oxidized form. Confocal microscopy analysis revealed that RPE cells exposed to high glucose exhibited increased green fluorescence signals, indicating higher levels of reduced C11-BODIPY and elevated lipid peroxidation. Conversely, these cells showed a less intense red fluorescence signal, indicating reduced levels of the oxidized form (Fig. 4B). However, pretreatment with TE-GNPs limited the increase in lipid peroxidation, as evidenced by the reduced green fluorescence intensity and increased red fluorescence signal in high glucose-exposed RPE cells. Collectively, our results indicate that exposure to high glucose leads to lipid accumulation and peroxidation in RPE cells, contributing to an aging phenotype. Treatment with TE-GNPs effectively mitigated these processes, providing relief from cellular aging associated with lipid accumulation and peroxidation.

4. Discussion

The green synthesis of nanoparticles using plant extracts has emerged as a promising alternative to conventional chemical

methods. Plant extracts contain various biomolecules that can serve as reducing agents to transform metal ions into nanoscale materials. This green synthesis approach offers several advantages, such as simplicity, energy efficiency, and cost-effectiveness, making it suitable for large-scale production. In this study, we utilized TE extract, which is rich in natural carotenoids with antioxidant properties, for the synthesis of TE-GNPs. The successful synthesis of TE-GNPs was confirmed through comprehensive physicochemical characterization, demonstrating their desirable properties such as strong antioxidative activity, nanoscale size, stability, crystallinity, and well-defined morphology (Shreyash et al., 2021b, Guo et al., 2020, Marouzi et al., 2021). The potential applications of TE-GNPs were explored in the context of diabetic eye diseases, specifically DR, which is characterized by dysfunction and damage to the RPE due to hyperglycemia-induced oxidative stress. The roles of cellular senescence, lipid metabolism, and oxidative stress in RPE dysfunction and the pathogenesis of DR are not fully understood but have been implicated in contributing to cellular senescence and disruption of lipid homeostasis (Nolan et al., 2021, Seo et al., 2019, Lima et al., 2022). Understanding these processes is crucial for developing effective therapeutic strategies. In this study, we aimed to investigate the effects of TE-GNPs on RPE cells cultured under high glucose conditions to better understand the underlying mechanisms of RPE dysfunction in DR and explore the potential therapeutic applications of TE-GNPs. We found that TE-GNPs were biocompatible and did not significantly affect RPE cell viability, indicating their safety for potential use in therapeutic interventions. Importantly, under high glucose conditions, the proliferation rate of RPE cells was restored upon treatment with TE-GNPs, suggesting their potential protective

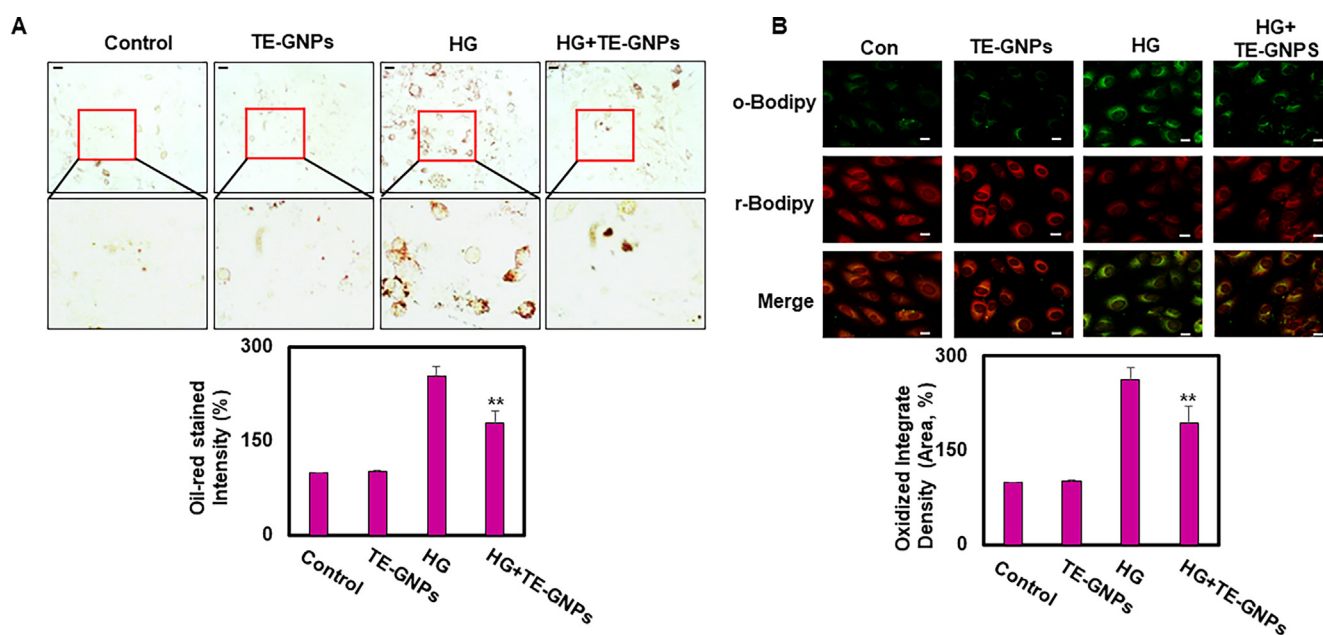


Fig. 4 Effects of TE-GNPs on lipid accumulation and lipid peroxidation in high glucose-cultured RPE Cells. (A) Representative images of Oil Red O staining showing extent of lipid accumulation in RPE cells. (B) Visualization of lipid peroxidation levels using BODIPY-581/591 C11 probe via confocal microscopy. Images were captured using 40x water-immersion objective. Data are presented as mean \pm standard error (SE) of three independent experiments, and statistical significance is indicated by ## $p < 0.05$ and ** $p < 0.01$.

effect against high glucose-induced RPE damage. These findings provide valuable insights into the potential application of TE-GNPs for the management of DR. Furthermore, we observed an increase in apoptotic or dying cells in RPE cells exposed to high glucose, which was significantly reduced by treatment with TE-GNPs. This indicates that TE-GNPs have the potential to mitigate cell death induced by high glucose, highlighting their protective effect against RPE damage. Oxidative stress is known to play a critical role in retinal damage, and we investigated the intracellular production of ROS in RPE cells. High glucose exposure led to increased ROS levels, indicating oxidative damage. However, treatment with TE-GNPs resulted in a significant reduction in intracellular ROS levels, suggesting their potential as antioxidants. Additionally, high glucose-exposed RPE cells exhibited elevated mitochondrial ROS levels, which were significantly reduced after TE-GNP treatment, indicating a potential mitigation of mitochondrial ROS generation. These findings further support the antioxidative properties of TE-GNPs and their potential to counteract oxidative stress-induced damage in RPE cells. Cellular senescence is associated with various molecular and phenotypic changes, and we explored its role in RPE dysfunction. Our results revealed that RPE cells exposed to high levels of glucose exhibited enhanced senescence, as evidenced by increased SA- β -gal activity. However, pretreatment with TE-GNPs significantly reduced SA- β -gal activity, indicating their ability to inhibit cellular senescence. Lysosomal dysfunction is another hallmark of cellular senescence, and we investigated its association with high glucose-induced RPE senescence. High glucose exposure led to increased lysosomal content in RPE cells, but pretreatment with TE-GNPs effectively reduced lysosomal content, suggesting their potential in mitigating lysosomal dysfunction associated with cellular senescence. Furthermore, to investigate whether RPE cells respond to high

glucose levels by accumulating lipids, we conducted Oil Red O staining to detect neutral lipids stored within lipid droplets. RPE cells exposed to high glucose exhibited increased lipid accumulation, as indicated by the intensity of Oil Red O staining. However, pretreatment with TE-GNPs significantly reduced lipid accumulation in RPE cells exposed to high glucose, suggesting their potential in reducing lipid accumulation. Lipid peroxidation, which contributes to cellular senescence, was assessed using a BODIPY-581/591 C11 probe. RPE cells exposed to high glucose showed increased lipid peroxidation, which was limited by TE-GNPs, as evidenced by reduced levels of oxidized lipids.

5. Conclusion

This study highlights the potential of TE-GNPs synthesized using marigold extract as a promising approach for mitigating RPE damage caused by high glucose-induced oxidative stress in DR. The TE-GNPs exhibited biocompatibility, restored RPE cell proliferation, reduced cell death, decreased intracellular ROS levels, and inhibited cellular senescence. Furthermore, they effectively reduced lipid accumulation and peroxidation in RPE cells exposed to high glucose concentrations. These findings demonstrate the advantages of utilizing green synthesis methods and natural plant extracts in nanoparticle synthesis, offering sustainable and eco-friendly alternatives. The remarkable anti-senescence effects, stability, and antioxidant properties of TE-GNPs make them promising candidates for future biomedical applications.

Declaration of Competing Interest

The authors declare that they have no known competing financial interests or personal relationships that could have appeared to influence the work reported in this paper.

Acknowledgments

This research was supported by the Basic Science Research Program of the National Research Foundation of Korea (NRF) funded by the Ministry of Education, Science, and Technology (NRF-2018R1D1A1B07047497 and NRF-2021R1I1A3A04035369).

References

- Ali, A., Zafar, H., Zia, M., ul Haq, I., Phull, A.R., Ali, J.S., Hussain, A., 2016. Synthesis, characterization, applications, and challenges of iron oxide nanoparticles. *Nanotechnology, science and applications*, 49-67.
- Al-Radadi, N.S., 2021. Facile one-step green synthesis of gold nanoparticles (AuNp) using licorice root extract: Antimicrobial and anticancer study against HepG2 cell line. *Arab. J. Chem.* 14, 102956.
- Anwar, Y., Ullah, I., Ul-Islam, M., Alghamdi, K.M., Khalil, A., Kamal, T., 2021. Adopting a green method for the synthesis of gold nanoparticles on cotton cloth for antimicrobial and environmental applications. *Arab. J. Chem.* 14, 103327.
- Chen, Q., Tang, L.I., Xin, G., Li, S., Ma, L., Xu, Y., Zhuang, M., Xiong, Q., Wei, Z., Xing, Z., 2019. Oxidative stress mediated by lipid metabolism contributes to high glucose-induced senescence in retinal pigment epithelium. *Free Radic. Biol. Med.* 130, 48–58.
- Fernández-Sevilla, J.M., Acién Fernández, F.G., Molina Grima, E., 2010. Biotechnological production of lutein and its applications. *Appl. Microbiol. Biotechnol.* 86, 27–40.
- Gansukh, E., Mya, K.K., Jung, M., Keum, Y., Kim, D.H., Saini, R. K., 2019. Lutein derived from marigold (*Tagetes erecta*) petals triggers ROS generation and activates Bax and caspase-3 mediated apoptosis of human cervical carcinoma (HeLa) cells. *Food Chem. Toxicol.* 127, 11–18.
- Guo, Y., Jiang, N., Zhang, L., Yin, M., 2020. Green synthesis of gold nanoparticles from *Fritillaria cirrhosa* and its anti-diabetic activity on Streptozotocin induced rats. *Arab. J. Chem.* 13, 5096–5106.
- Hassan, H., Sharma, P., Hasan, M.R., Singh, S., Thakur, D., Narang, J., 2022. Gold nanomaterials—The golden approach from synthesis to applications. *Materials Science for Energy Technologies*.
- Jeevanandam, J., Kiew, S.F., Boakye-Ansah, S., Lau, S.Y., Barhoum, A., Danquah, M.K., Rodrigues, J., 2022. Green approaches for the synthesis of metal and metal oxide nanoparticles using microbial and plant extracts. *Nanoscale* 14, 2534–2571.
- Kouhpanji, M.R.Z., Stadler, B.J.H., 2020. A guideline for effectively synthesizing and characterizing magnetic nanoparticles for advancing nanobiotechnology: A review. *Sensors (Basel)* 20, 2554. <https://doi.org/10.3390/s20092554>.
- Lee, K.S., Lin, S., Copland, D.A., Dick, A.D., Liu, J., 2021. Cellular senescence in the aging retina and developments of senotherapies for age-related macular degeneration. *J. Neuroinflamm.* 18, 1–17.
- Lee, E.J., Won, J.P., Lee, H.G., Kim, E., Hur, J., Lee, W.J., Hwang, J. S., Seo, H.G., 2022. PPAR δ inhibits hyperglycemia-triggered senescence of retinal pigment epithelial cells by upregulating SIRT1. *Antioxidants* 11, 1207.
- Lima, J.E., Moreira, N.C., Sakamoto-Hojo, E.T., 2022. Mechanisms underlying the pathophysiology of type 2 diabetes: From risk factors to oxidative stress, metabolic dysfunction, and hyperglycemia. *Mutation Res./Genet. Toxicol. Environ. Mutagen.* 874, 503437.
- Madhavan, J., Chandrasekharan, S., Priya, M.K., Godavarthi, A., 2018. Modulatory effect of carotenoid supplement constituting Lutein and Zeaxanthin (10:1) on anti-oxidant enzymes and macular pigments level in rats. *Pharmacogn Mag.* 14, 268–274.
- Marouzi, S., Sabouri, Z., Darroudi, M., 2021. Greener synthesis and medical applications of metal oxide nanoparticles. *Ceram. Int.* 47, 19632–19650.
- Meurer, M., de Oliveira, B.M.M., Cury, B.J., Jerônimo, D.T., Venzon, L., França, T.C.S., Mariott, M., Silva-Nunes, R., Santos, A.C., Roman-Junior, W.A., Oliveira, R.G., Arunachalam, K., Santin, J. R., Benvenutti, L., Souza, P., Aldana-Mejía, J.A., da Silva, L., 2022. Extract of *Tagetes erecta* L., a medicinal plant rich in lutein, promotes gastric healing and reduces ulcer recurrence in rodents. *J. Ethnopharmacol.* 293, 115258.
- Meurer, M.C., Mees, M., Mariano, L.N.B., Boeing, T., Somensi, L.B., Mariott, M., da Silva, Rita de Cássia Melo Vilhena de Andrade Fonseca, Dos Santos, A.C., Longo, B., Santos França, T.C., Klein-Júnior, L.C., de Souza, P., de Andrade, S.F., da Silva, L.M., 2019. Hydroalcoholic extract of *Tagetes erecta* L. flowers, rich in the carotenoid lutein, attenuates inflammatory cytokine secretion and improves the oxidative stress in an animal model of ulcerative colitis. *Nutr. Res.* 66, 95-106.
- Nolan, N.D., Jenny, L.A., Wang, N., Tsang, S.H., 2021. Retinal pigment epithelium lipid metabolic demands and therapeutic restoration. *Taiwan J. Ophthalmol.* 11, 216.
- Patil, S., Chandrasekaran, R., 2020. Biogenic nanoparticles: a comprehensive perspective in synthesis, characterization, application and its challenges. *J. Genet. Eng. Biotechnol.* 18, 67-020-00081-3.
- Prakash, M., Kavitha, H.P., Abinaya, S., Vennila, J.P., Lohita, D., 2022. Green synthesis of bismuth based nanoparticles and its applications-A review. *Sustain. Chem. Pharm.* 25, 100547.
- Ren, C., Hu, C., Wu, Y., Li, T., Zou, A., Yu, D., Shen, T., Cai, W., Yu, J., 2022. Nicotinamide Mononucleotide Ameliorates Cellular Senescence and Inflammation Caused by Sodium Iodate in RPE. *Oxidative Medicine and Cellular Longevity* 2022.
- Rodrigues, S.M., Demokritou, P., Dokoozlian, N., Hendren, C.O., Karn, B., Mauter, M.S., Sadik, O.A., Safarpour, M., Unrine, J.M., Viers, J., 2017. Nanotechnology for sustainable food production: promising opportunities and scientific challenges. *Environ. Sci. Nano* 4, 767–781.
- Salem, S.S., Hammad, E.N., Mohamed, A.A., El-Dougdoug, W., 2022. A comprehensive review of nanomaterials: Types, synthesis, characterization, and applications. *Biointerface Res. Appl. Chem* 13, 41.
- Sampath, S., Madhavan, Y., Muralidharan, M., Sunderam, V., Lawrance, A.V., Muthupandian, S., 2022. A review on algal mediated synthesis of metal and metal oxide nanoparticles and their emerging biomedical potential. *J. Biotechnol.* 360, 92–109.
- Sarfraz, N., Khan, I., 2021. Plasmonic gold nanoparticles (AuNPs): properties, synthesis and their advanced energy, environmental and biomedical applications. *Chem.–Asian J.* 16, 720–742.
- Selvaraj, R., Pai, S., Vinayagam, R., Varadavenkatesan, T., Kumar, P. S., Duc, P.A., Rangasamy, G., 2022. A recent update on green synthesized iron and iron oxide nanoparticles for environmental applications. *Chemosphere* 308, 136331.
- Seo, E., Kang, H., Choi, H., Choi, W., Jun, H., 2019. Reactive oxygen species-induced changes in glucose and lipid metabolism contribute to the accumulation of cholesterol in the liver during aging. *Aging Cell* 18, e12895.
- Shamarao, N., Chethankumar, M., 2022. Antiobesity drug-likeness properties and pancreatic lipase inhibition of a novel low molecular weight lutein oxidized product, LOP6. *Food Funct.* 13, 6036–6055.
- Shreyash, N., Bajpai, S., Khan, M.A., Vijay, Y., Tiwary, S.K., Sonker, M., 2021a. Green synthesis of nanoparticles and their biomedical applications: A review. *ACS Appl. Nano Mater.* 4, 11428–11457.
- Shreyash, N., Bajpai, S., Khan, M.A., Vijay, Y., Tiwary, S.K., Sonker, M., 2021b. Green synthesis of nanoparticles and their biomedical applications: A review. *ACS Applied Nano Materials* 4, 11428-11457.

- Tan, L.X., Germer, C.J., La Cunza, N., Lakkaraju, A., 2020. Complement activation, lipid metabolism, and mitochondrial injury: Converging pathways in age-related macular degeneration. *Redox Biol.* 37, 101781.
- Tang, H., Du, H., Kuang, X., Huang, H., Zeng, J., Long, C., Zhu, B., Fu, L., Wang, H., Zhang, Q., 2022. Arbutin protects retinal pigment epithelium against oxidative stress by modulating SIRT1/FOXO3a/PGC-1 α / β pathway. *Front. Genet.* 13, 1763.
- Tohari, A.M., Almarhoun, M., Alhasani, R.H., Biswas, L., Zhou, X., Reilly, J., Zeng, Z., Shu, X., 2020. Protection by vitamin D against high-glucose-induced damage in retinal pigment epithelial cells. *Exp. Cell Res.* 392, 112023.
- Wang, M., Tsao, R., Zhang, S., Dong, Z., Yang, R., Gong, J., Pei, Y., 2006. Antioxidant activity, mutagenicity/anti-mutagenicity, and clastogenicity/anti-clastogenicity of lutein from marigold flowers. *Food Chem. Toxicol.* 44, 1522–1529.
- Zhang, H., Zhang, S., Zhang, H., Chen, X., Liang, F., Qin, H., Zhang, Y., Cong, R., Xin, H., Zhang, Z., 2020. Carotenoid metabolite and transcriptome dynamics underlying flower color in marigold (*Tagetes erecta* L.). *Sci. Rep.* 10, 16835-020-73859-7.